Analytical and Bioanalytical Chemistry
https://doi.org/10.1007/s00216-021-03567-2

RESEARCH PAPER

Enzymatic electrochemical biosensor for glyphosate detection based on acid phosphatase inhibition

Preeyanut Butmee[1] · Gamolwan Tumcharern[1] · Chomphunuch Songsiriritthigul[2,3] · Marie José Durand[4] · Gerald Thouand[4] · Margaret Kerr[5] · Kurt Kalcher[6] · Anchalee Samphao[7,8]

Received: 17 June 2021 / Revised: 16 July 2021 / Accepted: 19 July 2021

Abstract

A novel enzymatic electrochemical biosensor was fabricated for the indirect detection of glyphosate-based acid phosphatase inhibition. The biosensor was constructed on a screen-printed carbon electrode modified with silver nanoparticles, decorated with electrochemically reduced graphene oxide, and chemically immobilized with acid phosphatase via glutaraldehyde cross-linking. We measured the oxidation current by chronoamperometry. The current arose from the enzymatic reaction of acid phosphatase and the enzyme-substrate disodium phenyl phosphate. The biosensing response is a decrease in signal resulting from inhibition of acid phosphatase in the presence of glyphosate inhibitor. The inhibition of acid phosphatase by glyphosate was investigated as a reversible competitive-type reaction based on the Lineweaver-Burk equation. Computational docking confirmed that glyphosate was the inhibitor bound in the substrate-binding pocket of acid phosphatase and that it was able to inhibit the enzyme efficiently. Additionally, the established method was applied to the selective analysis of glyphosate in actual samples with satisfactory results following a standard method.

Keywords Glyphosate · Electrochemical biosensor · Acid phosphatase · Graphene oxide · Silver nanoparticles

Introduction

Glyphosate [N-(phosphonomethyl)glycine], classified in a group of organophosphorus pesticides, is one of the more extensively used herbicides in agriculture worldwide. The compound has lower toxicity to mammals compared to other pesticides [1]. However, glyphosate residues in agricultural products present a health hazard to humans and have led to environmental contaminations [2, 3]. Moreover, glyphosate contains carcinogenic contaminants and causes DNA and organ damage [4]. Glyphosate was determined to be a potential carcinogen to humans (group 2A) by the International Agency for Research on Cancer in 2015. Many responsible authorities have selected the maximum residue levels (MRLs) of glyphosate in water, soil, and agricultural products [5]. For example, the maximum contaminant level of glyphosate in water and soil is set as 0.7 μg mL^{-1} and 2 mg kg^{-1}, respectively, by the World Health Organization (WHO), and the MRLs in most crops reported by the United Nations Food and Agricultural Organization (FAO) are 0.1–5.0 mg kg^{-1}

✉ Gamolwan Tumcharern
gamolwan@nanotec.or.th

✉ Anchalee Samphao
anchalee.s@ubu.ac.th

[1] National Nanotechnology Center, National Science and Technology Development Agency, Pathumthani 12120, Thailand

[2] Synchrotron Light Research Institute (Public Organization), 111 University Avenue, Nakhon Ratchasima 30000, Thailand

[3] Center for Biomolecular Structure, Function and Application, Suranaree University of Technology, Nakhon Ratchasima 30000, Thailand

[4] Nantes Université, ONIRIS, CNRS, GEPEA, UMR 6144, F-85000 La Roche sur Yon, France

[5] Department of Chemistry, Worcester State University, 486 Chandler Street, Worcester, MA 01602, United States

[6] Institute of Chemistry-Analytical Chemistry, University of Graz, A-8010, Graz, Austria

[7] Department of Chemistry, Faculty of Science, Ubon Ratchathani University, Ubon Ratchathani 34190, Thailand

[8] Department of Chemistry and Center of Excellence for Innovation in Chemistry, Faculty of Science, Ubon Ratchathani University, Ubon Ratchathani 34190, Thailand

Published online: 27 July 2021

[6, 7]. Therefore, to increase public health and food security, there is a need to develop a rapid, reliable, and sensitive approach for analyzing glyphosate in environmental samples to provide an early warning in contamination incidents.

Various analytical methods have been reported for glyphosate determination. These methods include high-performance liquid chromatography (HPLC) [8, 9], gas chromatography coupled with mass spectrometry (GC-MS) [10], capillary electrophoresis [11], and fluorescence [12], colorimetric [6], spectrophotometric [13], and electrochemical methods [2, 7, 14]. Electrochemical techniques can offer a rapid, simplistic, sensitive, and selective analysis. Therefore, various analytical strategies based on electrochemical biosensors have been designed and used as efficient alternative devices for detecting glyphosate. However, glyphosate is a non-electroactive herbicide that cannot be detected by direct electrochemical methods [15]. Using enzyme inhibition is a popular method used for ultra-sensitive herbicide detection. In addition, enzyme inhibition biosensors offer a popular method for the fast and straightforward detection of toxic compounds such as pesticides and metal ions.

Typically, enzyme inhibition biosensor-based acetylcholinesterase (AChE) has been employed as an enzyme receptor to detect organophosphorus pesticides indirectly [16]. However, there are major drawbacks to using AChE. Several compounds, such as glyphosate, carbamate pesticides, aflatoxins, nerve agents, and heavy metals [17], can specifically inhibit the activity of the AChE enzyme. Therefore, selecting an appropriate enzyme to serve as the bioreceptor is necessary to produce a highly selective and sensitive biosensor. To our knowledge, acid phosphatase (ACP), a family of hydrolase enzymes, could be applied for quantitative measurement of glyphosate due to its function in catalyzing the hydrolysis of phosphoric acid-containing molecules [18, 19]. The ACP catalyzes the hydrolysis of its substrate, disodium phenyl phosphate, into phenol and phosphoric acid (Eq. 1). The produced phenol is then oxidized to benzoquinone (Eq. 2), which can be measured with different electrochemical transducers. The ACP inhibition is detected by measuring the decreased oxidation current of the phenol products due to the phosphoric group in the glyphosate structure as the competitive inhibitor, thus inhibiting ACP activity.

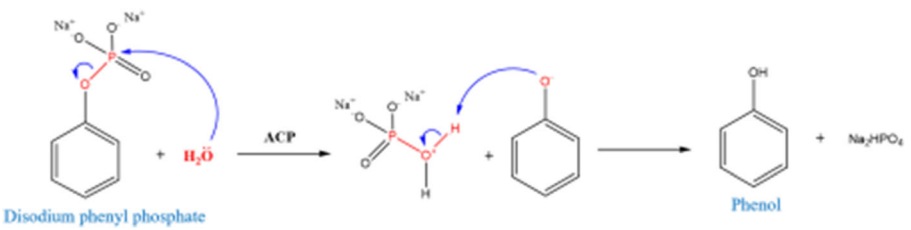

(1)

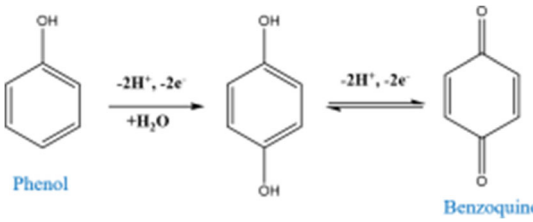

(2)

However, ACP faces lower sensitivity than the AChE inhibition methods. Therefore, many nanomaterials, especially graphene nanomaterials and metal nanoparticles, have gained popularity for the fabrication of electrochemical biosensors and improve sensitivity to inhibit signal detection. For example, silver nanoparticles (AgNPs) are among the most frequently used metal nanomaterials for signal enhancement in a wide range of electrochemical biosensing applications. This is because silver has a large surface-to-volume ratio, good electrical properties, unique catalytic properties, excellent biocompatibility, and lower cost than other materials [20–22]. Additionally, incorporating AgNPs with graphene nanomaterials could boost electron transfer rate of electrochemical biosensing as a consequence from a large π-π conjugations in graphene structure compared to using single AgNPs component [23–25].

This research describes the design of a novel enzymatic electrochemical biosensor showing ACP inhibition by glyphosate. The designed biosensor is constructed by electrodeposition of AgNPs and electrochemically reduced graphene oxide (ErGO) at the active electrode surface of screen-printed carbon electrode (SPCE) for indirect measurement of glyphosate in order to receive a portable and disposable biosensor that is suitable for on-field analysis. The ACP is chemically immobilized on the modified biosensing area via glutaraldehyde cross-linking, denoted as SPCE/ErGO-AgNPs/GA-ACP. The oxidation current signal due to the enzymatic reaction of ACP and disodium phenyl phosphate is measured at a constant potential by chronoamperometry. Therefore, a decrease in signal response resulting from inhibition of ACP activity in the glyphosate inhibitor correlates with the glyphosate concentration.

Moreover, molecular docking of the optimized bound conformations and the binding free energy of ligands to enzymes [26] plausibly explains the reduced enzymatic activity of ACP, thus supporting the developed system for indirect measurement of glyphosate. This strategy has been demonstrated

to be applicable for the sensitive and selective analysis of glyphosate in environmental samples.

Materials and methods

Chemicals and reagents

Glyphosate (PESTANAL®, analytical standard), acid phosphatase (ACP, phosphatase acid type I from wheat germ, 0.5 unit mg^{-1} solid), disodium phenyl phosphate dibasic dihydrate ($C_6H_5Na_2O_4P.2H_2O$), glutaraldehyde (GA, grade II, 25% in H_2O), graphene oxide (GO powder, 15–20 sheets, 4–10% edge-oxidized), silver nitrate ($AgNO_3$, ACS reagent, ≥99.0%), 4-chloro-3,5-dinitrobenzotrifluoride (CNBF, 98%), and formic acid (CH_2O_2, ACS reagent, ≥96.0%) were obtained from Sigma-Aldrich. Carbon ink (carbon paste, C2030519P4) and silver/silver chloride ink (Ag/AgCl paste 60:40, C2130809D5) were obtained from Sun Chemicals (UK). Acetate buffer adjusted to various pH values was used as a supporting electrolyte, prepared by mixing acetic acid and sodium acetate solutions. All other chemicals were of analytical reagent grade and purchased from Sigma-Aldrich. Ultrapure water (18.2 MΩ cm) obtained from the Milli-Q cartridge system was used throughout. Dilution of working solutions and samples was carried out before use.

Apparatus and materials

The AgNPs-ErGO nanocomposites were analyzed by X-ray diffraction spectroscopy (XRD, X'Pert-MPD, PHILIPS, Netherlands) using a Cu source over a range of diffraction angles 2 = 10–80°, and Raman spectroscopy performed on a Labspec6-Horiba Raman spectrophotometer (1024X256-OE, Raman Instruments Inc. Edison, USA) equipped with a microscope (100× objective lens) and laser source at 532 nm. The morphology of SPCE modified with AgNPs-ErGO and covered with ACP-GA was investigated by a field emission scanning electronic microscope (FE-SEM, JSM-7610FPlus, JEOL, USA), coupled with an energy-dispersive X-ray spectrometer (EDS, X-MAX IE-350, Oxford, UK). All electrochemical measurements were carried out using a computer-controlled electrochemical workstation (Autolab, PGSTAT302N, Metrohm, Switzerland) with the NOVA software suite installed (version *1*.11).

Electrochemical biosensor fabrication

We fabricated the SPCEs by manually printing the commercial carbon ink and Ag/AgCl ink onto a transparent projector film (PVC) through the block screen (constructed by Silkcut LP, Thailand). The SPCE consists of a pseudo-Ag/AgCl reference electrode (RE), a carbon counter electrode (CE), and a carbon working electrode (WE). First, an insulator layer was painted using clear nail polish, which was adhered to the conductive pad to prevent the spread of the test solution. Then, 10 μL of GO droplet dispersed in deionized water was deposited onto the active surface of the working electrode. After 30 min of drying, a mixed solution of 0.1 M KNO_3 solution containing $AgNO_3$ and 0.1 M sodium acetate was injected onto the SPCE surface. The co-reduction of GO and Ag was achieved by scanning the potential from 0.0 to −1.2 V with cyclic voltammetry (CV) at a scan rate of 50 mV/s for 10 cycles. After electrodeposition, the obtained SPCE/ErGO-AgNPs was washed with deionized water and gently dried under an N_2 flow at room temperature. Finally, 5 μL of ACP enzyme was cast onto the modified electrode by cross-linking with 5% glutaraldehyde to obtain the enzymatic biosensor. Figure 1a shows the fabrication process of the SPCE/ErGO-AgNPs/GA-ACP biosensor. Figure 1b is a schematic illustration of the working principle of an electrochemical biosensor based on enzyme activity and enzyme inhibition.

Molecular docking of ACP enzyme

From the X-ray crystal structure of acid phosphatase from red kidney bean (PDB code 4KBP), the dimeric protein-containing Fe (III) and Zn(II) complexed with phosphate ion represent the catalytic site in wheat germ [27]. Two docked ligands downloaded from PubChem (https://pubchem.ncbi.nlm.nih.gov) as structural data files were subsequently formatted with structural coordinates using eLBOW [28]. The coordinates of disodium phenyl phosphate substrate and glyphosate were initially docked into the enzyme active site using *AutoDock Vina* [26]. Finally, the structures were generated using the PyMOL molecular graphics system [29].

Sample preparation

Glyphosate-contaminated water and soil samples were extracted following a previous method with minor modifications [1, 2]. First, environmental water (50 mL) was sonicated for 15 min, followed by filtration using a 0.45-μm nylon membrane filter. Then, 1.0 mM $Ba(OH)_2$ was added to the collected supernatants and sonicated. Next, sulfate radical and most metal ions were eliminated by centrifugation at 10,000 rpm for 10 min. Next, the pH of the resulting supernatants was adjusted with 1 M HCl to maintain the samples at pH 7.0. Finally, the extracted samples were separated by centrifugation at 10,000 rpm for a further 10 min. The final solutions were freeze-dried and stored at −20°C for further use.

NaOH (1 M, 60 mL) was added to 25 g of the soil samples and continuously stirred for 30 min with a magnetic stirrer. The sample mixtures were centrifuged for 10 min at 5000 rpm, and the collected supernatants were

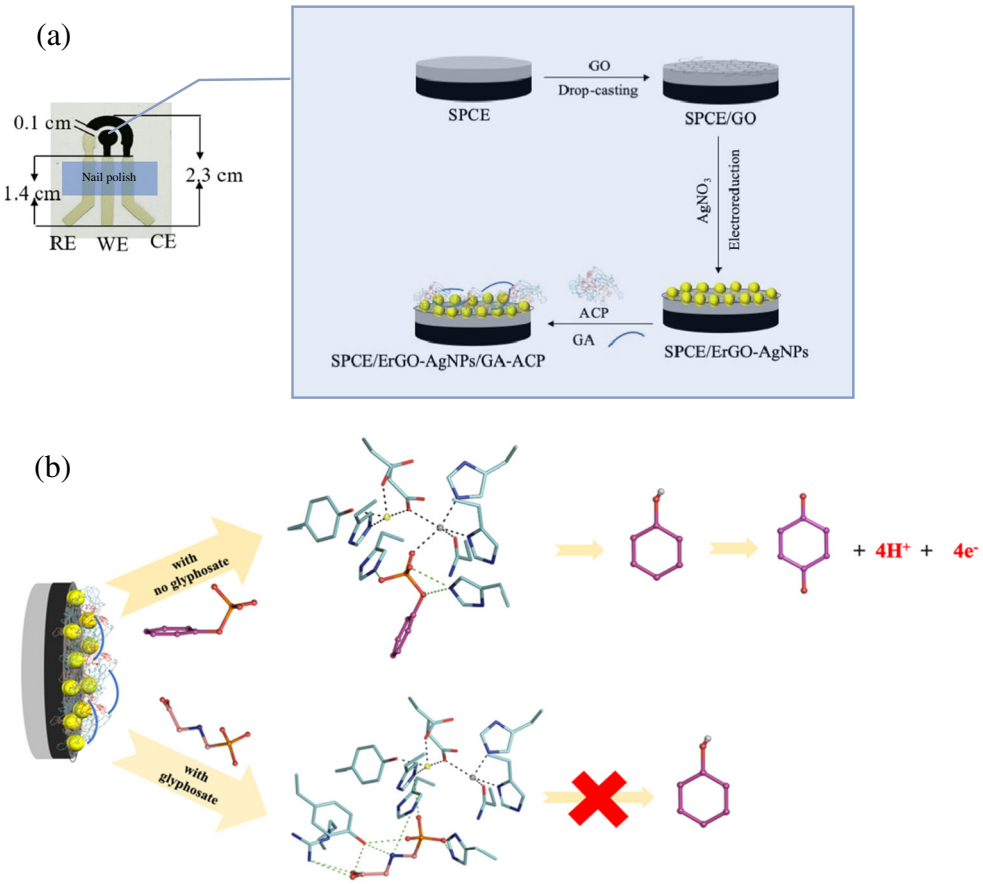

Fig. 1 A schematic of (**a**) bare SPCE and SPCE/ErGO-AgNPs/GA-ACP fabrication and (**b**) acid phosphatase catalysis with disodium phenyl phosphate with glyphosate inhibition

subsequently filtered with a-0.45 μm nylon membrane filter. After that, the supernatants were brought to pH 7.0 with 1 M HCl and then centrifuged at 5000 rpm for a further 10 min. The extracted samples were diluted in distilled water, made up to 100 ml, freeze-dried, and kept at −20°C for further use.

Chromatographic conditions

The amount of glyphosate contaminant in environmental waters and soils was analyzed by a standard ultra-high-performance liquid chromatography (UHPLC) method to confirm the reliability of the proposed biosensor. The quantitative analysis of glyphosate was achieved after derivatization with 4-chloro-3,5-dinitrobenzotrifluoride (CNBF) [3]. The UHPLC separation of derivative glyphosate was performed on a C18 column (2.1 × 50 mm, 1.8 μm, Zorbax, Agilent) under a flow rate of 0.2 mL min^{-1}, a detection wavelength of 360 nm, an injection volume of 15 μL, and a column temperature of 40°C. The solution mixture of acetonitrile and 0.2% formic acid was used as the HPLC mobile phase. The elution gradient programs were set from 5% to reach 100% of acetonitrile in 10 min.

Results and discussion

Characterization of the SPCE/ErGO-AgNPs/GA-ACP biosensor

The crystalline nature of the SPCE/ErGO-AgNPs was verified by X-ray diffraction (XRD) analysis. Figure 2a compares the experimental XRD patterns of the bare SPCE and ErGO-modified SPCE. The SPCE exhibits a sharp X-ray diffraction peak at $2\theta = 26.5°$, agreeing with the (002) plane of the typical crystal structure of graphite [30]. There is no significant difference in the XRD profile for ErGO-modified SPCE. The characteristic GO peak at 2θ of 11.0° was not observed [31], indicating that GO was reduced entirely to ErGO. After AgNPs deposition, the prominent peaks located at 2θ = 38.2°, 44.4°, 66.6°, and 78.5° are related to (111), (200), (220), and (311) crystallographic orientation planes of the face-centered cubic (FCC) structure of silver (JCPDS No. 04-0783) [32].

The modifications on the SPCE surface with ErGO-AgNPs nanocomposites were validated by Raman spectroscopy (Fig. 2b). The Raman bands at 1351 cm^{-1} and 1588 cm^{-1}, attributed to sp^3 and sp^2 hybridization of carbon materials, termed D and G bands [31], are present in all conditions. Typically, the D and G peak intensities (I_D/I_G) are used to estimate the degree of structural defects in the

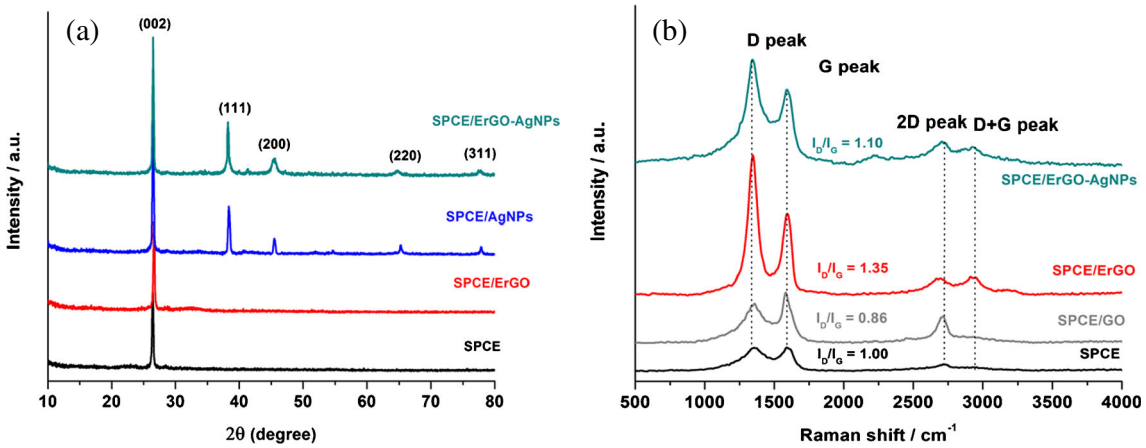

Fig. 2 (**a**) XRD patterns and (**b**) Raman spectra of the SPCE and SPCE modified with different nanomaterials

carbon material [33]. The I_D/I_G ratio decreased from 1.00 to 0.86 after GO modification of the SPCE since the GO contributes to increased sp^2 carbon bonds [34]. On the other hand, the ratio of I_D/I_G increased to 1.35 and 1.10 after introducing ErGO and ErGO-AgNPs on the SPCE surface, respectively. Thus, more defects in the graphitized structure are created to remove C=O bonds during the electrochemical reduction process [31].

Furthermore, the characteristic Raman peak at around 2700 cm^{-1}, known as the secondary D peak or the 2D band, is detected. The intensity ratio between the 2D and G peaks (I_{2D}/I_G) is generally used to determine the graphene layer [35]. For example, the SPCE/ErGO-AgNPs exhibits an I_{2D}/I_G ratio of 0.8, suggesting that a few layers of ErGO were covered on the surface of the electrode. Additionally, the elemental compositions of the modified electrode were studied using energy-dispersive spectroscopy (EDS) (see Supplementary Information Fig. S1).

Figure 3 shows the surface morphologies of the enzymatic biosensor observed by field emission scanning electron microscopy (FE-SEM). The bare SPCE consists of a flake-like morphology and a spherical structure of carbon. A thin, wrinkled layered structure of ErGO, and globular AgNPs, having an average diameter of about 150 nm, is detected after the electrochemical deposition procedure. The noticeable changes in the morphology of the modified electrode are observed after loading of GA-linked ACP enzyme, providing evidence of successful enzyme immobilization.

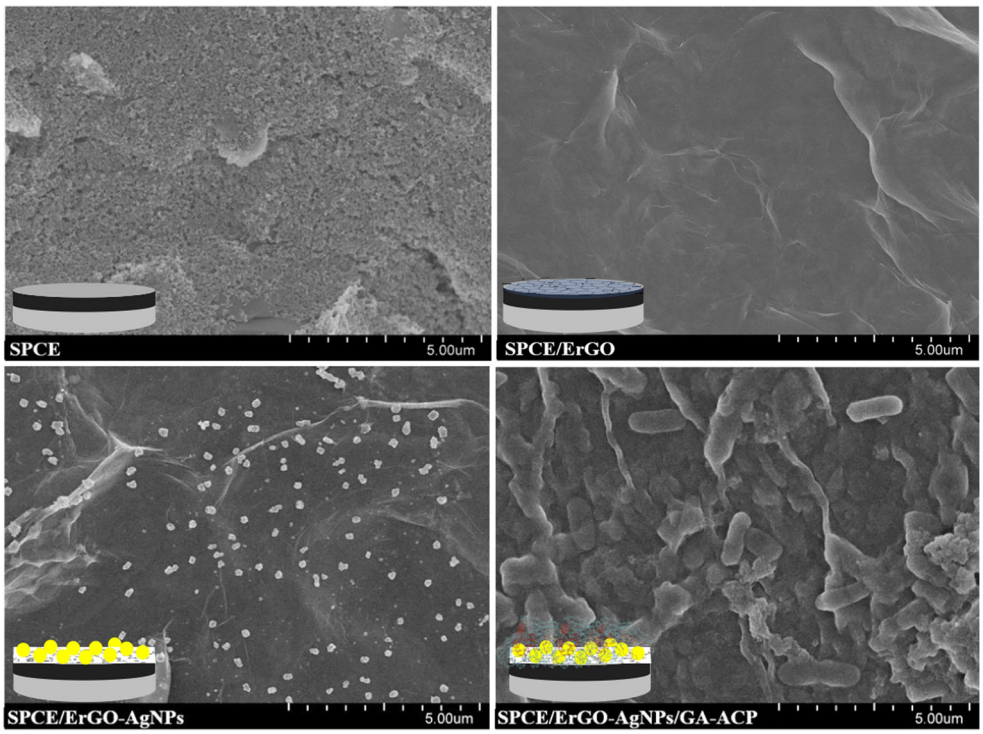

Fig. 3 FE-SEM images of different modified SPCEs

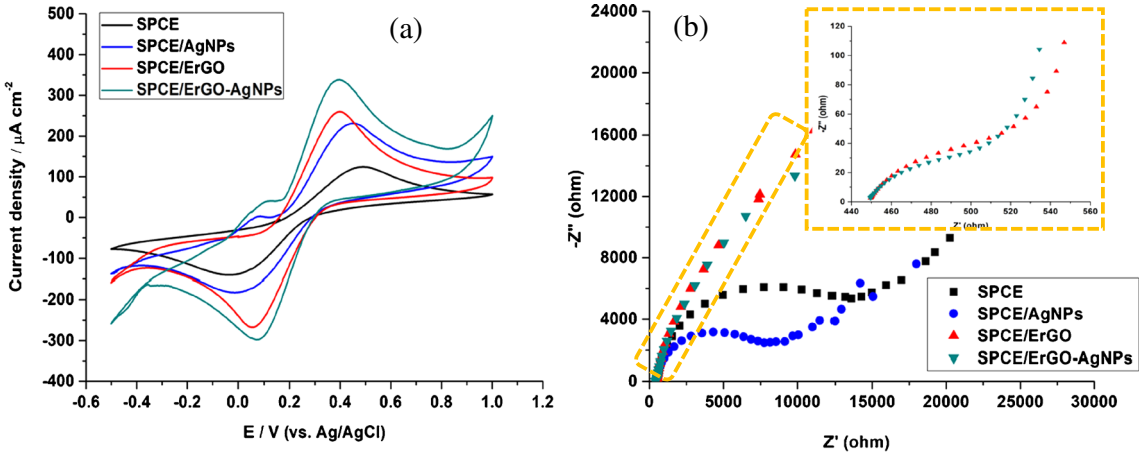

Fig. 4 (**a**) CVs and (**b**) EIS signals of different modified electrodes in 1 mM $Fe(CN)_6^{3-/4-}$ solution (inset: the EIS signals compared between SPCE/ErGO and SPCE/ErGO-AgNPs)

Electrochemical characterizations of the modified electrodes

Cyclic voltammetry (CV) was carried out in 1 mM $Fe(CN)_6^{3-/4-}$ solution to investigate the characteristic electrochemical properties of the prepared SPCE/ErGO-AgNPs. Figure 4a displays the voltammograms of unmodified and modified SPCE with AgNPs, ErGO, and ErGO-AgNPs. The symmetric redox peaks of $Fe(CN)_6^{3-/4-}$ were observed in all conditions, indicating reversible redox reactions. Furthermore, a weak redox peak was received on the bare SPCE, in which an oxidative current density (J_p) of 123.6 μA cm^{-2} and a peak-to-peak separation (ΔE_p) of 0.59 V were obtained. After modifying SPCE with AgNPs and ErGO, the J_p increased but the ΔE_p

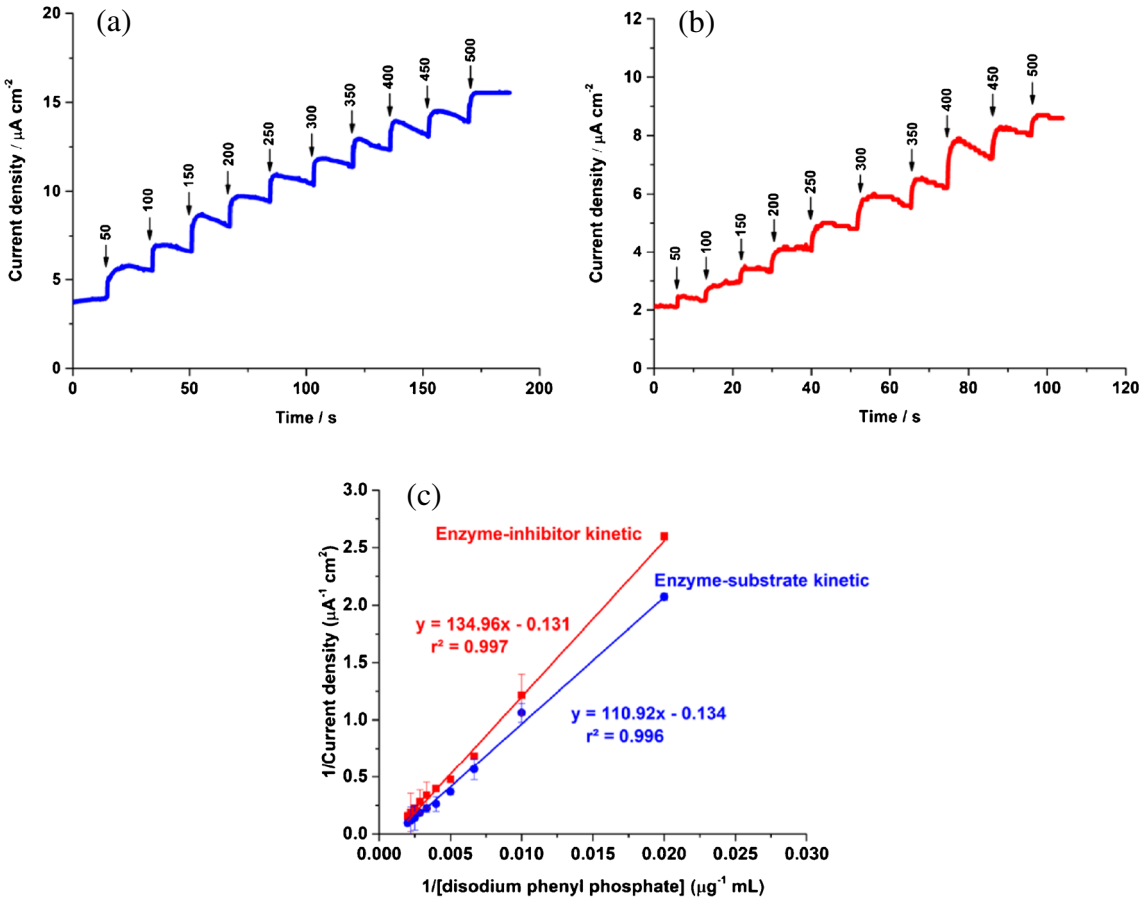

Fig. 5 Amperometric response of the SPCE/ErGO-AgNPs/GA-ACP to successive injections of 50–500 μg mL^{-1} disodium phenyl phosphate in acetate buffer (pH 7.0) in the (**a**) absence and (**b**) presence of 1 μg mL^{-1} glyphosate, and (**c**) corresponding to Lineweaver-Burk plots

decreased compared to the unmodified bare SPCE. Thus, AgNPs and ErGO nanomaterials can help enhance electrical conductivity and acceleration of the electron transfer process of the electrode [36]. Apart from $Fe(CN)_6^{3-/4-}$, the electrochemical performance of the SPCE/ErGO-AgNPs was investigated for phenol detection (see Supplementary Information Fig. S2).

For further characterization of the electrochemical interface features of the prepared SPCE/ErGO-AgNPs, electrochemical impedance spectroscopy (EIS) was employed (Fig. 4b). It is seen that a semicircle portion of the EIS signal related to charge transfer resistance (R_{ct}) decreased after modification with AgNPs, due to the excellent electrical conductivity of the Ag metal. On the other hand, the R_{ct} value was dramatically reduced for ErGO-modified SPCE, confirming that the large π-π conjugations in the ErGO structure could reform the electrode to more sensitive charge transfer and reduce surface resistance [37]. The lowest R_{ct} on the SPCE modified with AgNPs and ErGO reveals the synergistic contribution of the advantages from those two nanomaterials.

Enzyme inhibition kinetic study

The response of the electrochemical biosensor to variable concentrations of disodium phenyl phosphate was detected by chronoamperometry under optimized conditions. Figure 5a and b show the typical amperometric current-time response for the SPCE/ErGO-AgNPs/GA-ACP biosensor in the absence and presence of 1 μg mL^{-1} glyphosate, respectively. Without glyphosate, the biosensor with the added disodium phenyl phosphate exhibited an oxidation current. Meanwhile, less sensitive current responses were recorded in the presence of glyphosate. Based on these results, a Lineweaver-Burk plot was plotted for $1/I$ versus $1/C$ (Fig. 5c). The kinetic constants, K_m and V_{max}, were then determined by fitting a linear function and analyzing the slope and intercept in the Lineweaver-Burk plot. The K_m and V_{max} were calculated, with no glyphosate, to be 3.79 mM and 7.46 μA cm^{-2}. The obtained K_m was close to the value (3.5 mM) reported by Zhang et al. [38]. In the presence of glyphosate, the K_m and V_{max} values were estimated to be 4.72 mM and 7.63 μA cm^{-2}, respectively. This observation

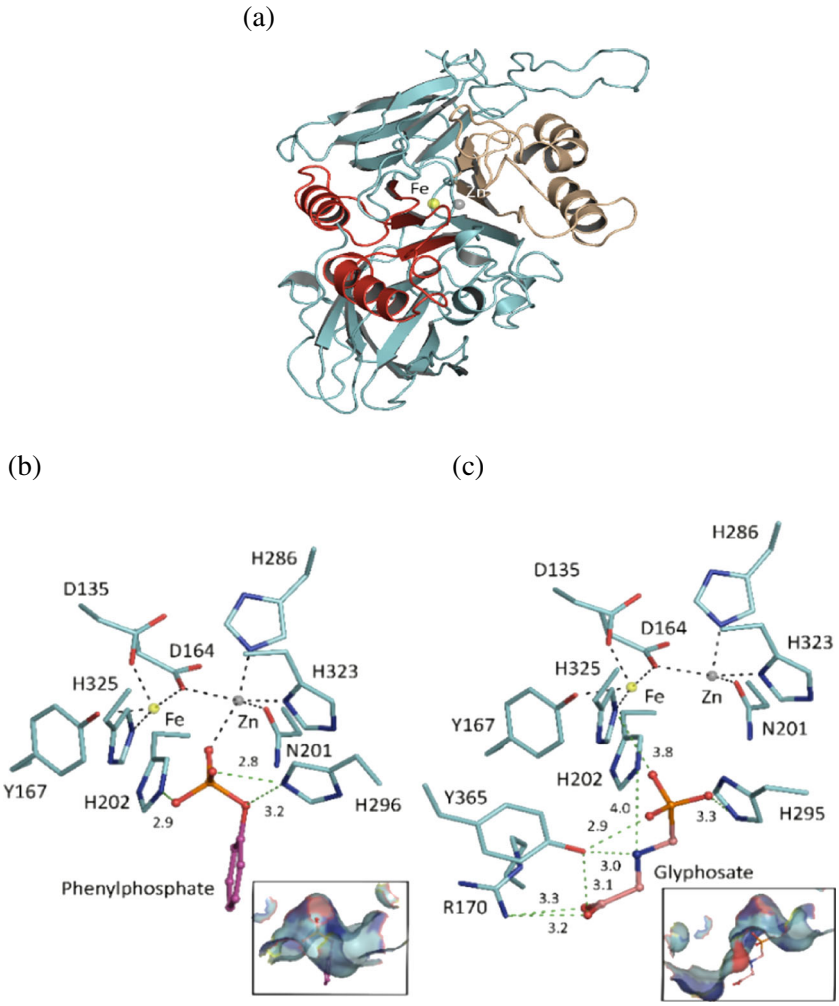

Fig. 6 (**a**) The overall structure of ACP from red kidney bean (PDB entry 4KBP), (**b**) phenyl phosphate docked, and (**c**) glyphosate docked

shows that the inhibition of ACP activity by glyphosate increases the K_m value, whilst the V_{max} value remained almost the same. Therefore, the inhibitory effect of glyphosate on the SPCE/ErGO-AgNPs/GA-ACP biosensor is a reversible competitive type. In addition to kinetic study, the electrochemical behavior of the biosensor dependent on the scan rate was examined (see Supplementary Information Fig. S3).

Computational docking study

The structures of modelled ligands, including disodium phenyl phosphate and glyphosate, bound in the ACP enzyme structure were studied to understand better the accommodation of these two ligands in the catalytic site of the ACP from wheat germ. There were not any previous reports revealing the X-ray structure of ACP from wheat, specifically. Therefore, the crystal structure of ACP from red kidney bean (PDB entry 4KBP) has been representatively studied in this work since the ACP from wheat and red kidney bean are both classified in the same group of the ACP family [39]. Figure 6a reveals that the X-ray structure of ACP from red kidney bean comprises of two sandwiched βαβαβ motifs which form the core unit of metal coordinating. The dimeric protein-containing Fe(III) and Zn(II) represent the catalytic site in wheat germ in this study [26, 40].

The docking study of phenyl phosphate into the X-ray structure of ACP is shown in Fig. 6b. One oxygen atom of the phosphate group is within covalent bonding distance to the Zn ion (2.3 Å). Two oxygen atoms of the phosphate group have hydrogen bonds at His202 and His296 with lengths of 2.9 Å and 2.8 Å, respectively. The side chain of His296 is at a hydrogen-bonding distance of 3.2 Å, with an esterified oxygen atom as the leaving group for the hydrolysis of the enzyme. The optimized conformation of phenyl phosphate has a binding free energy of −4.7 kcal mol^{-1}.

Docking studies of glyphosate (Fig. 6c) show that the metal ions are further away from the phosphate group. However, three oxygen atoms of the phosphate group are hydrogen-bonded to His295, His325, and Tyr365, with distances of 3.3 Å, 3.8 Å, and 2.9 Å, respectively. The nitrogen atom of glyphosate is hydrogen-bonded (4.0 Å) with the imidazole side chain of His202. The phenolic side chain of Tyr365 is hydrogen-bonded at a distance of 3.0 Å. Moreover, two carboxylate groups are assumed to form hydrogen bonds with the guanidino side chain of Arg170 (3.2 Å and 3.3 Å). Notably, one carboxylate of bound glyphosate is oriented for a hydrogen bond interaction at a distance of 3.1 Å from Tyr365, located in the active site of the ACP enzyme. The stabilized conformation of glyphosate yields binding free energy of −4.9 kcal mol^{-1}, which is slightly lower than the value of phenyl phosphate. Thus, the orientation of glyphosate in the substrate-binding pocket is optimized by hydrogen bonds, supporting the binding preference of glyphosate, thus efficiently inhibiting the ACP activity in hydrolyzing phenyl phosphate.

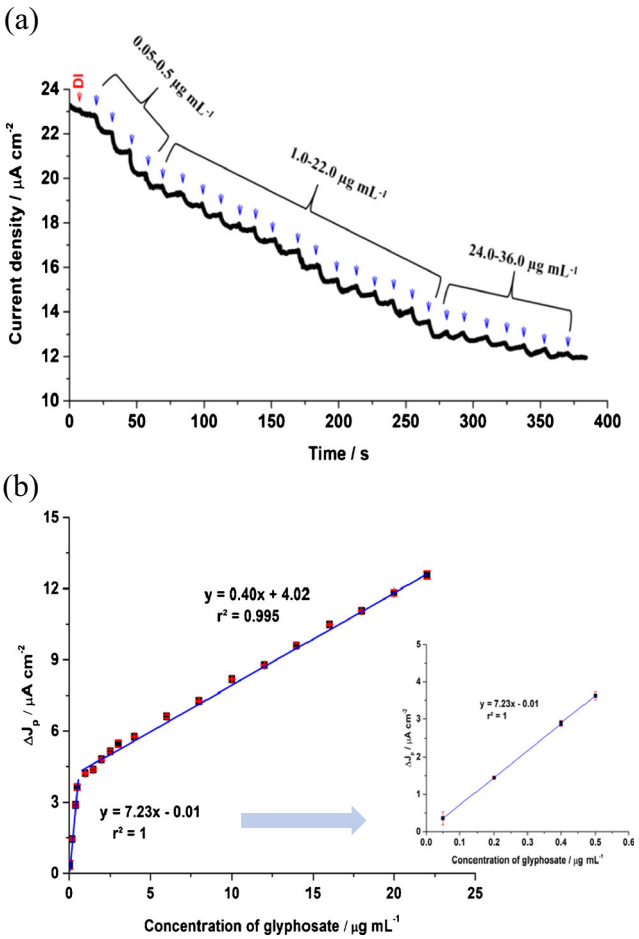

Fig. 7 (**a**) Amperometric response of the SPCE/ErGO-AgNPs/GA-ACP for indirect detection of glyphosate and (**b**) its calibration plots from 0.05 to 0.5 μg mL^{-1} and from 0.5 to 22.0 μg mL^{-1}

Analytical performances of the enzymatic biosensor

The linearity of the SPCE/ErGO-AgNPs/GA-ACP biosensor for indirect determination of glyphosate herbicide was studied by chronoamperometry under optimal conditions (see details in Supplementary Information Fig. S4). The amperometric current-time curve of the proposed ACP biosensor is successively reduced in series with added glyphosate solution at various concentrations (Fig. 7a). This result showed in a decrease in enzymatic function due to reversible binding between the glyphosate and the active site of the ACP enzyme. The calibration curve (Fig. 7b) shows that the inhibited current density signals (ΔJ_p) linearly increased with higher glyphosate concentration, in which two linear ranges were obtained, from 0.05 to 0.5 μg mL^{-1} and from 0.5 to 22.0 μg mL^{-1}. The higher inhibitor concentration provided a lower enzymatic activity towards its substrate. The decrease of enzyme response in the calibration plot from 0.5 to 22.0 μg mL^{-1} showed the inhibition response

in decreasing order when glyphosate concentration was increased. A very high inhibitor concentration reversibly occupied most active sites, but not all glyphosate molecules were consistently bound to the enzyme. The greater inhibitor concentration provided a lower inhibition effect.

The detection limit (LOD) and quantification limit (LOQ) were calculated at 0.015 μg mL^{-1} and 0.045 μg mL^{-1}, respectively, based on 3SD/slope and 10SD/slope. SD is the standard deviation of glyphosate detected at the lowest concentration from the linear range and the slope obtained from the low-range calibration curve. The obtained LOD value was below the maximum contaminant levels of glyphosate in drinking water (0.7 μg mL^{-1}) and soil (2 mg kg^{-1}) recommended by the WHO [6]. It is also lower than the MRLs of glyphosate in most crops (0.1–5.0 mg kg^{-1}), as suggested by the FAO [7]. Therefore, the proposed SPCE/ErGO-AgNPs/GA-ACP possessed greater sensitivity than prior research adopted (Table S1).

Reproducibility, stability, and selectivity

The intra-day and inter-day reproducibility of the SPCE/ErGO-AgNPs/GA-ACP for detection (0.2 μg mL^{-1} glyphosate) was evaluated by using five different electrodes (n=5). The relative standard deviation (RSD) was calculated at 5.21% and 5.46% for intra-day and inter-day tests, respectively. Furthermore, the stability of the prepared biosensor was investigated. During the first 5 days of storage, the amperometric responses of the biosensor remained at more than 81.9% of its initial signal. However, after a week of storage, a rapid decrease in signal was observed, resulting from reducing enzyme activity and denaturation of ACP during the long-term storage [41]. Additionally, selectivity of the developed biosensor was examined (see Supplementary Information Fig. S5).

Real sample analysis

The amount of glyphosate contaminating environmental water and soil samples was determined by the SPCE/ErGO-AgNPs/GA-ACP biosensor to check the practical reliability of the ACP biosensor. The experiments were performed in triplicate by the standard addition method range from 0 to 0.3 μg mL^{-1} as shown in Fig. S6a and the standard addition plot depicted in Fig. S6b. Furthermore, the accuracy and precision of the biosensor were investigated using recovery measurements on spiked samples. As demonstrated in Table 1, the average recoveries of 95.6–104.7% upon spiking were received. These

Table 1 Determination of glyphosate in environmental waters and soils by the enzymatic biosensor and UHPLC (n=3)

Sample	Added		Determined by the biosensor			Determined by UHPLC			t-testb
			Measured		Recovery (%)	Measured		Recovery (%)	
	(μg g^{-1})	(μg mL^{-1})	(μg g^{-1})	(μg mL^{-1})		(μg g^{-1})	(μg mL^{-1})		
Water A		-		n.d.[a]	-		n.d.	-	-
		0.5		0.50 ± 0.05	100.1		0.52 ± 0.01	103.4	0.7
		1.0		1.04 ± 0.12	104.0		1.04 ± 0.03	103.8	0.1
Water B		-		n.d.	-		n.d.	-	-
		0.5		0.51 ± 0.03	102.4		0.52 ± 0.01	103.2	0.2
		1.0		1.02 ± 0.07	102.1		0.96 ± 0.03	96.1	2.1
Water C		-		n.d.	-		n.d.	-	-
		0.5		0.50 ± 0.03	100.8		0.49 ± 0.01	98.4	0.9
		1.0		1.05 ± 0.12	104.7		0.96 ± 0.03	95.9	1.0
Soil A	0		0.66 ± 0.06		-	0.79 ± 0.01		-	2.1
	2.0		2.64 ± 0.24		99.3	2.76 ± 0.10		98.6	0.5
	4.0		4.48 ± 0.32		95.6	4.74 ± 0.16		98.7	0.9
Soil B	-		n.d.		-	n.d.		-	-
	2.0		2.08 ± 0.10		104.0	2.05 ± 0.09		102.6	0.3
	4.0		4.05 ± 0.20		101.3	4.13 ± 0.16		103.1	0.5
Soil C	-		n.d.		-	n.d.		-	-
	2.0		2.08 ± 0.06		104.1	2.00 ± 0.06		100.2	0.4
	4.0		3.89 ± 0.27		97.2	4.01 ± 0.08		100.3	0.6

[a] n.d. means "not detectable"

[b] t-test at a confidence level of 95% probability and degree of freedom of 2

results indicated that the developed SPCE/ErGO-AgNPs/GA-ACP biosensor was reliable for indirectly detecting glyphosate herbicide in environmental samples.

Additionally, the feasibility of the proposed biosensor was tested by detecting glyphosate contaminated in the water and soil samples by UHPLC as a comparative standard method. Finally, the concentration of glyphosate in actual samples was analyzed in triplicate by an external calibration plot. The results agreed well with the results reported from the electrochemical biosensor. There were no significant differences between the two methods, owing to a smaller *t*-value than the tabulated critical value at a degree of freedom of 2 and a confidence interval of 95% probability.

Conclusions

In this work, a proposed strategy for glyphosate herbicide detection depended on enzyme inhibition was presented. An acid phosphatase biosensor was developed based on immobilization of ACP via glutaraldehyde cross-linking on the active area of a screen-printed carbon electrode modified with silver nanoparticles decorated with electrochemically reduced graphene oxide. The oxidative current signals were obtained from an enzymatic reaction between the acid phosphatase enzyme and its substrate disodium phenyl phosphate measured by chronoamperometry. A decrease in the obtained signal in the presence of glyphosate resulted from reversible competitive inhibition, based on the Lineweaver-Burk equation. Furthermore, the inhibitory effect was studied computationally by a docking approach. It was demonstrated that glyphosate was well oriented in the active site pocket of acid phosphatase. It was able to efficiently inhibit the catalytic enzyme function in the presence of phenyl phosphate substrate.The designed biosensor exhibited two linear ranges for glyphosate from 0.05 to 0.5 μg mL^{-1} (r^2 = 0.995) and from 0.5 to 22.0 μg mL^{-1} (r^2 = 0.995) with a detection limit and a quantification limit of 0.015 μg mL^{-1} and 0.045 μg mL^{-1}, respectively. The proposed biosensor also achieved excellent reproducibility, stability, and selectivity. It was practically introduced to the selective electrochemical analysis of glyphosate in the environmental water and soil samples with excellent recoveries. Furthermore, the results were in accordance with a standard UHPLC method as evaluated by *t*-test at a confidence interval of 95% probability.

Supplementary Information The online version contains supplementary material available at https://doi.org/10.1007/s00216-021-03567-2.

Acknowledgements This research was supported by National Nanotechnology Center (NANOTEC); National Science and Technology Development Agency (NSTDA); Faculty of Science, Ubon Ratchathani University (Thailand); the Center of Excellence for Innovation in Chemistry (PERCH-CIC); and Office of the Higher Education Commission, Ministry of Education (OHEC), Thailand. In particular, A.S. and K.K. would gratefully thank the ASEAN-European Academic University Network (ASEA-UNINET); the Austrian Federal Ministry of Education, Science and Research; and the Austrian Agency for International Mobility and Cooperation in Education, Science and Research (OeAD-GmbH) for their joint support.

Funding The research was granted by Thailand Graduate Institute of Science and Technology (TGIST grant No. TG-55-24-60-010D).

Declarations

Conflict of interest The authors declare no competing interests.

References

1. Wang L, Bi Y, Hou J, Li H, Xu Y, Wang B, et al. Facile, green and clean one-step synthesis of carbon dots from wool: application as a sensor for glyphosate detection based on the inner filter effect. Talanta. 2016;160:268–75.
2. Gholivand MB, Akbari A, Norouzi L. Development of a novel hollow fiber-pencil graphite modified electrochemical sensor for the ultra-trace analysis of glyphosate. Sens Actuators B Chem. 2018;272:415–24.
3. Gil PM, Laguarda-Miro N, Camino JS, Peris RM. Glyphosate detection with ammonium nitrate and humic acids as potential interfering substances by pulsed voltammetry technique. Talanta. 2013;115:702–5.
4. Zhan H, Feng Y, Fan X, Chen S. Recent advances in glyphosate biodegradation. Appl Microbiol Biotechnol. 2018;102(12):5033–43.
5. Jiménez-López J, Llorent-Martínez EJ, Ortega-Barrales P, Ruiz-Medina A. Graphene quantum dots-silver nanoparticles as a novel sensitive and selective luminescence probe for the detection of glyphosate in food samples. Talanta. 2020;207:120344.
6. De Almeida LKS, Chigome S, Torto N, Frost CL, Pletschke BI. A novel colorimetric sensor strip for the detection of glyphosate in water. Sens Actuators B Chem. 2015;206:357–63.
7. Prasad BB, Jauhari D, Tiwari MP. Doubly imprinted polymer nanofilm-modified electrochemical sensor for ultra-trace simultaneous analysis of glyphosate and glufosinate. Biosens Bioelectron. 2014;59:81–8.
8. Sun L, Kong D, Gu W, Guo X, Tao W, Shan Z, et al. Determination of glyphosate in soil/sludge by high performance liquid chromatography. J Chromatogr A. 2017;1502:8–13.
9. Wang S, Liu B, Yuan D, Ma JA. A simple method for the determination of glyphosate and aminomethylphosphonic acid in seawater matrix with high performance liquid chromatography and fluorescence detection. Talanta. 2016;161:700–6.
10. Motojyuku M, Saito T, Akieda K, Otsuka H, Yamamoto I, Inokuchi SJ. Determination of glyphosate, glyphosate metabolites, and glufosinate in human serum by gas chromatography–mass spectrometry. J Chromatogr B. 2008;875(2):509–14.
11. Chiu HY, Lin ZY, Tu HL, Whang CWJ. Analysis of glyphosate and aminomethylphosphonic acid by capillary electrophoresis with electrochemiluminescence detection. J Chromatogr A. 2008;1177(1):195–8.
12. Yuan Y, Jiang J, Liu S, Yang J, Yan J, Hu X. Fluorescent carbon dots for glyphosate determination based on fluorescence resonance energy transfer and logic gate operation. Sens Actuators B Chem. 2017;242:545–53.

13. Çetin E, Şahan S, Ülgen A, Şahin U. DLLME-spectrophotometric determination of glyphosate residue in legumes. Food Chem. 2017;230:567–71.
14. Cao Y, Wang L, Shen C, Wang C, Hu X, Wang G. An electrochemical sensor on the hierarchically porous Cu-BTC MOF platform for glyphosate determination. Sens Actuators B Chem. 2019;283:487–94.
15. Kurbanoglu S, Ozkan SA, Merkoci A. Nanomaterials-based enzyme electrochemical biosensors operating through inhibition for biosensing applications. Biosens Bioelectron. 2017;89:886–98.
16. Songa EA, Okonkwo JO. Recent approaches to improving selectivity and sensitivity of enzyme-based biosensors for organophosphorus pesticides: a review. Talanta. 2016;155:289–304.
17. Amine A, Arduini F, Moscone D, Palleschi G. Recent advances in biosensors based on enzyme inhibition. Biosens Bioelectron. 2016;76:180–94.
18. Lin Z, Zhang X, Liu S, Zheng L, Bu Y, Deng H, et al. Colorimetric acid phosphatase sensor based on MoO_3 nanozyme. Anal Chim Acta. 2020;1105:162–8.
19. Li S, Hu X, Chen Q, Zhang X, Chai H, Huang Y. Introducing bifunctional metal-organic frameworks to the construction of a novel ratiometric fluorescence sensor for screening acid phosphatase activity. Biosens Bioelectron. 2019;137:133–9.
20. Shoja Y, Kermanpur A, Karimzadeh F, Ghodsi J, Rafati AA, Adhami S. Electrochemical molecularly bioimprinted siloxane biosensor on the basis of core/shell silver nanoparticles/EGFR exon 21 L858R point mutant gene/siloxane film for ultra-sensing of Gemcitabine as a lung cancer chemotherapy medication. Biosens Bioelectron. 2019;145:111611.
21. Nantaphol S, Chailapakul O, Siangproh W. Sensitive and selective electrochemical sensor using silver nanoparticles modified glassy carbon electrode for determination of cholesterol in bovine serum. Sens Actuators B Chem. 2015;207:193–8.
22. Chen M, Wang Y, Su H, Mao L, Jiang X, Zhang T, et al. Three-dimensional electrochemical DNA biosensor based on 3D graphene-Ag nanoparticles for sensitive detection of CYFRA21-1 in non-small cell lung cancer. Sens Actuators B Chem. 2018;255:2910–8.
23. Santos AM, Wong A, Fatibello-Filho O. Simultaneous determination of salbutamol and propranolol in biological fluid samples using an electrochemical sensor based on functionalized-graphene, ionic liquid and silver nanoparticles. Electroanal Chem. 2018;824:1–8.
24. Huang KJ, Wang L, Wang HB, Gan T, Wu YY, Li J, et al. Electrochemical biosensor based on silver nanoparticles-polydopamine-graphene nanocomposite for sensitive determination of adenine and guanine. Talanta. 2013;114:43–8.
25. Shah A, Malik MS, Zahid A, Iftikhar FJ, Anwar A, Akhter MS, et al. Carbamazepine coated silver nanoparticles for the simultaneous electrochemical sensing of specific food toxins. Electrochim Acta. 2018;274:131–42.
26. Trott O, Olson AJJ. AutoDock Vina: improving the speed and accuracy of docking with a new scoring function, efficient optimization, and multithreading. J Comput Chem. 2010;31(2):455–61.
27. Klabunde T, Sträter N, Fröhlich R, Witzel H, Krebs BJ. Mechanism of Fe (III)-Zn (II) purple acid phosphatase based on crystal structures. J Mol Biol. 1996;259(4):737–48.
28. Moriarty NW, Grosse-Kunstleve RW, Adams PD. Electronic Ligand Builder and Optimization Workbench (eLBOW): a tool for ligand coordinate and restraint generation. Acta Crystallographica Section D Biological Crystallography. 2009;65(10):1074–80.
29. DeLano WL. The PyMOL Molecular Graphics System. DeLano Scientific LLC: USA; 2002.
30. Atacan KJ. $CuFe_2O_4$/reduced graphene oxide nanocomposite decorated with gold nanoparticles as a new electrochemical sensor material for -cysteine detection. J Alloys Compd. 2019;791:391–401.
31. Oghli AH, Soleymanpour A. Polyoxometalate/reduced graphene oxide modified pencil graphite sensor for the electrochemical trace determination of paroxetine in biological and pharmaceutical media. Mater Sci Eng C. 2020;108:110407.
32. Satyanarayana M, Goud KY, Reddy KK, Kumar VS, Gobi KV. Silver nanoparticles impregnated chitosan layered carbon nanotube as sensor interface for electrochemical detection of clopidogrel in-vitro. Mater Sci Eng C. 2019;101:103–10.
33. Zeng Y, Zhou Y, Zhou T, Shi G. A novel composite of reduced graphene oxide and molecularly imprinted polymer for electrochemical sensing 4-nitrophenol. Electrochim Acta. 2014;130:504–11.
34. Moreira LFPP, Buffon E, Stradiotto NR. Electrochemical sensor based on reduced graphene oxide and molecularly imprinted poly (phenol) for D-xylose determination. Talanta. 2020;208:120379.
35. Lin JC, Huang BR, Lin TC. Hybrid structure of graphene sheets/ZnO nanorods for enhancing electron field emission properties. Appl Surf Sci. 2014;289:384–7.
36. Jin H, Guo H, Gao X, Gui R. Selective and sensitive electrochemical sensing of gastrodin based on nickel foam modified with reduced graphene oxide/silver nanoparticles complex-encapsulated molecularly imprinted polymers. Sens Actuators B Chem. 2018;277:14–21.
37. Yu S, Jiang Y, Wang C. A polymer composite consists of electrochemical reduced graphene oxide/polyimide/chemical reduced graphene oxide for effective preparation of SnSe by electrochemical atomic layer deposition method with enhanced electrochemical performance and surface area. Electrochim Acta. 2013;114:430–8.
38. Zhang J, Yuan Y, Han Z, Li Y, van Zijl PC, Yang X, et al. Detecting acid phosphatase enzymatic activity with phenol as a chemical exchange saturation transfer magnetic resonance imaging contrast agent (PhenolCEST MRI). Biosens Bioelectron. 2019;141:111442.
39. Zhu S, Chen M, Liang C, Xue Y, Lin S, Tian J. Characterization of purple acid phosphatase family and functional analysis of GmPAP7a/7b involved in extracellular ATP utilization in soybean. Front Plant Sci. 2020;11:661.
40. Schenk G, Elliott TW, Leung E, Carrington LE, Mitić N, Gahan LR, et al. Crystal structures of a purple acid phosphatase, representing different steps of this enzyme's catalytic cycle. BMC Struct Biol. 2008;8(1):1–13.
41. Jiang Y, Zhang X, Pei L, Yue S, Ma L, Zhou L, et al. Silver nanoparticles modified two-dimensional transition metal carbides as nanocarriers to fabricate acetylcholinesterase-based electrochemical biosensor. Chem Eng J. 2018;339:547–56.